Potential energy surfaces for $N = Z$, ^{20}Ne–^{112}Ba nuclei

M S MEHTA[*], T K JHA[†], S K PATRA[‡] and RAJ K GUPTA[*]

[*]Physics Department, Panjab University, Chandigarh 160 014, India
[†]Department of Physics, Sambalpur University, Jyoti Vihar, Burla 768 019, India
[‡]Institute of Physics, Sachivalaya Marg, Bhubaneswar 751 005, India
E-mail: patra@iopb.res.in

Abstract. We have calculated the potential energy surfaces for $N = Z$, ^{20}Ne–^{112}Ba nuclei in an axially deformed relativistic mean field approach. A quadratic constraint scheme is applied to determine the complete energy surface for a wide range of the quadrupole deformation. The NL3, NL-RA1 and TM1 parameter sets are used. The phenomenon of (multiple) shape coextistence is studied and the calculated ground and excited state binding energies, quadrupole deformation parameters and root mean square (rms) charge radii are compared with the available experimental data and other theoretical predictions.

1. Introduction

In a recent work [1], we calculated the potential energy surfaces for some neutron-deficient $N = Z$ nuclei in the mass region $A \approx 80$. The phenomenon of multiple shape coexistence (more than two shapes at about the same binding energy) is predicted in this region, suggesting a 'dynamically' variable nature of the nuclear shapes in the neutron-deficient $N = Z$ exotic nuclei. Since the low level density in the nuclear potential of $A \approx 80$ mass region nuclei leads to the shell gaps in the nuclear mean field [2], the coexistence of neighbouring oblate and prolate shell gaps cause the nuclear deformation to change dramatically with the addition or subtraction of a few nucleons. This result is observed experimentally, i.e., with the addition of only two protons or two neutrons [3,4], the shape gets changed drastically and the low-lying isomeric states (two, coexisting nuclear shapes) become the ground band in this mass region [5]. In Nilsson–Strutinsky picture the shape coexistence can be understood as arising from the interplay between the liquid drop energy and the Nilsson single-particle energies [6]. The Nilsson single-particle energies depend

on the deformation, which results in more than one local minimum for the ground state total energy as a function of deformation [6].

There are many theoretical calculations available in the literature for calculating the potential energy surface (PES) diagram and to analyse the different structures of nuclei in different mass regions of the periodic table [6,7]. Earlier, using the dynamical deformation model (DDM), Kumar [8] predicted the shallow PES for Ge isotopes and showed strong collective effects in the deformation space as well as in the pairing interaction space. Wood *et al* [6] pointed out that in many cases the minima in 0-quasiparticle PES, even if they are very shallow and separated by very low energy barriers, correspond to well-defined states. They showed that, even the structures which do not correspond to a local minimum in PES may be closely related to the physical state of the nucleus, whose energy can be successfully extracted by removing spurious interactions with excited configurations. The number of particles occupying the single-particle intruder orbits can be treated as an additional quantum number. These observations suggest that a flat PES does not automatically lead to large fluctuations of shape. On the contrary, the nucleus may still be fairly rigid, the shape being restored not by a large energy barrier but by profound structural differences between different minima [6,7]. The studies of $N = Z$ nuclei in the mass region $A \simeq 60$–80 have also been reported using the Skyrme–Hartree–Fock (SHF) plus BCS method with a three-dimensional (3D) mesh representation [9,10] which show the existence of three (prolate, oblate and spherical) local minima. Takami *et al* [11] showed that, without imposing the requirement of symmetry on the solutions to allow arbitrary nuclear shapes, the reflection asymmetric shapes, violating the axial symmetry, are more favoured in $N = Z$ nuclei of mass region $A \simeq 60$–80 than with the axial symmetry. Recently, a superdeformed state with the quadrupole deformation parameter $\beta_2 = 0.65$ is also observed [12] in the $N = Z$, ^{36}Ar nucleus, which could also be an isomeric state, like in the mass region $A \approx 80$. This raises an apparent question: Do the shape coexisting states occur in all $N = Z$ nuclei beginning, say, from the normal ^{20}Ne nucleus to the very proton-rich ^{112}Ba nucleus lying almost at the proton-drip line? One of the aims of this work is to answer this question for the exotic $N = Z$ nuclei. It may be noted that the shape coexistence in neutron-deficient Pb isotopes were calculated by Bengtsson and Nazarewicz [7] using the configuration constrained shell correction method and they could separate the ground state PES into different parts. Recently, the multiple shape phenomenon is well-studied in Pb nuclei [13], where one of the best studied cases is ^{186}Pb. The three different-shaped (spherical, oblate and prolate) 0^+ states are also observed in the recent experiment at the SHIP of GSI [14].

The shape coexistence phenomenon provides information regarding the excitation energies of two (or more) neighbouring intrinsic states. Alternatively, this means that if deeper minima in the potential energy surface are not nearly equally deep (i.e. the energy difference between the first two minima $\Delta E > 2$–2.5 MeV), then such states are isomeric states, giving information about the first excited intrinsic state above the ground state (deepest minimum), and so on for the next minima. Since the first excited intrinsic state for *spherical* nuclei lie very high, it is possible that ΔE contains the information about the magic structure of nuclei and hence allows us to test the validity of model parameters used in, say, the mean field approaches

applied to nuclei far away from the valley of β-stability. The mean field models are often based on parameters derived from fits to stable or near-stable nuclei. This is another aim of the present investigation and we use here the axially deformed relativistic mean field (RMF) approach [15–18], with NL3, NL-RA1 and TM1 as the parameter sets. The potential energy surfaces are calculated in a quadratic constraint scheme [19–22], explained below.

The paper is organized as follows: Section 2 gives some very basic details concerning the relativistic mean field (RMF) formalism. The results of our calculations are presented in §3. The paper is concluded with a summary and discussion of our results in §4.

2. The relativistic mean field formalism

The relativistic mean field model is now a well-studied approach, where the relativistic Lagrangian density for a nucleon–meson many-body system is defined as [15–18],

$$
\begin{aligned}
\mathcal{L} = {} & \overline{\psi_i}\{i\gamma^\mu\partial_\mu - M\}\psi_i + \frac{1}{2}\partial^\mu\sigma\partial_\mu\sigma - \frac{1}{2}m_\sigma^2\sigma^2 - \frac{1}{3}g_2\sigma^3 - \frac{1}{4}g_3\sigma^4 - g_s\overline{\psi_i}\psi_i\sigma \\
& -\frac{1}{4}\Omega^{\mu\nu}\Omega_{\mu\nu} + \frac{1}{2}m_w^2 V^\mu V_\mu + \frac{1}{4}c_3(V_\mu V^\mu)^2 - g_w\overline{\psi_i}\gamma^\mu\psi_i V_\mu - \frac{1}{4}\vec{B}^{\mu\nu}\cdot\vec{B}_{\mu\nu} \\
& +\frac{1}{2}m_\rho^2\vec{R}^\mu\cdot\vec{R}_\mu - g_\rho\overline{\psi_i}\gamma^\mu\vec{\tau}\psi_i\cdot\vec{R}^\mu - \frac{1}{4}F^{\mu\nu}F_{\mu\nu} - e\overline{\psi_i}\gamma^\mu\frac{(1-\tau_{3i})}{2}\psi_i A_\mu.
\end{aligned} \tag{1}
$$

Here, the field for the σ-meson is denoted by σ, that of the ω-meson by V_μ and of the isovector ρ-meson by $\vec{R}_\mu$. A^μ denotes the electromagnetic field. ψ_i are the Dirac spinors for the nucleons, whose third component of isospin is denoted by τ_{3i}. g_s, g_w, g_ρ and $(e^2/4\pi) = (1/137)$ are the coupling constants for σ, ω, ρ mesons and the photon, respectively. g_2, g_3 and c_3 are the parameters for the non-linear terms of σ and ω mesons. M is the mass of the nucleon and m_σ, m_ω and m_ρ are the masses of the σ, ω and ρ mesons, respectively. $\Omega^{\mu\nu}$, $\vec{B}^{\mu\nu}$ and $F^{\mu\nu}$ are the field tensors for V^μ, $\vec{R}^\mu$ and the photon fields, respectively [16].

From the relativistic Lagrangian we get the field equations for the nucleons and the mesons. These equations are solved by expanding the upper and lower components of the Dirac spinors and the boson fields in a deformed harmonic oscillator basis with an initial deformation. The set of coupled equations is solved numerically by a self-consistent iteration method. The centre-of-mass motion is estimated by the usual harmonic oscillator formula $E_{\text{c.m.}} = \frac{3}{4}41A^{-1/3}$. The quadrupole deformation parameter β_2 is evaluated from the resulting quadrupole moment and the total binding energy and other observables are obtained by using the standard relations [16]. The $N_{\text{F}} = N_{\text{B}} = 12$ oscillator shells are used as the expansion basis for the fermion and boson fields.

In order to compute the whole potential energy surface, we introduce a quadrupole constraint, which means, instead of minimizing $\langle H \rangle$, we minimize $\langle H' \rangle$ where $\hat{H}' = \hat{H} - \mu\hat{Q}_\mu$, with $\hat{Q}_\mu = r^2 Y_{2\mu}(\theta, \phi)$ and the Lagrangian multiplier μ fixed by the constraint $\langle Q \rangle_\mu = Q_0$. In detail, we have solved the set of RMF equations

with two quadratic constraints [19,20]: $\frac{1}{2}C_0(\langle \hat{Q}_0 \rangle - \mu_0)^2 + \frac{1}{2}C_2(\langle \hat{Q}_2 \rangle - \mu_2)^2$, where the constraining operators $\hat{Q}_\mu$ are used as time components of a vector field in Dirac equation. The quadratic constraint is used in order to be able to treat also the concave areas of the energy surface [19,20]. The Lagrangian multiplier μ is adjusted to fix a definite deformation. It is to be noted here that, in nature, the triaxial degree of freedom is very important but triaxiality destroys the possibility of many isomers and allows a large amount of configuration mixing. In this way the violation of axial symmetry is possible [9–11]. Recently, exotic shapes (non-axial, with octupole deformations) and shape coexistence in $N = Z$ proton-rich nuclei from ^{64}Ge to ^{84}Mo by symmetry-unrestricted Skyrme–Hartree–Fock–Bogoliubov (Skyrme–HFB) methods have been reported [23], where the PES are calculated in constrained Skyrme-HFB approach. However, in the present calculation the triaxial degree of freedom is beyond the scope of our work. Therefore, we have restricted our calculation to an axially deformed RMF calculation only [19–22], termed as free calculations in order to distinguish them from the quadrupole constrained calculations.

3. Calculations and results

Our calculations are performed with the three successful parameter sets TM1 [24], NL3 [25] and NL-RA1 [26]. The predictive power of TM1 and NL3 parametrizations is well-known and some examples can be found, e.g., in ref. [27] and references quoted therein. The relatively new parameter set NL-RA1 is used recently in [28] and it is found that the results produced by this set are as good as that of the NL3. From the results presented in refs [26,28], it is evident that NL-RA1 can be considered successful and could be used with confidence for the fruitful investigations of the new regions of nuclear stability. On the other hand, an interesting feature of the TM1 is that, in this set the sign of the quartic scalar self-coupling is positive (contrary to that for NL3 and NL-RA1), which is achieved by introducing a quartic self-interaction of the vector field in the effective force [24,29]. It is worth mentioning that, the value of c_3 (eq. (1)) is non-zero in TM1 set, whereas it is zero in all other forces. Another significant difference is that the value of g_3 is positive in TM1 and it is negative in NL3, NL-SH and NL-RA1. In general, the quality of the results produced by TM1 is comparable to that of the standard non-linear NL3 and other parameter sets but so far it has not been used much in the literature. Although the TM1 parameter set is designed for $Z > 20$ nuclei, we have used it here for all the nuclei studied, for the sake of consistency. For the pairing energy, following the prescription of Madland and Nix [30], we have chosen to use the BCS formalism with the constant pairing gaps. Note that for most of the very neutron-deficient nuclei studied here, the odd–even mass differences are not measured, and hence very little is known about the precise effects of the pairing interactions. Also, it may be noted that the constant pairing strength, taken from experimental data or from the standard formula, fails to reproduce the quadrupole deformation of light nuclei like ^{20}Ne (the large experimental value of $\beta_2 = 0.72$ [31]), favouring no pairing strength [27]. In such cases, we use the constant gaps $\Delta_n = \Delta_p = 0.5$ MeV, and is called zero pairing. This type of prescription has already been adopted in

the past [32] taking $\Delta_n = \Delta_p = 0.5$ to 1 MeV and the chosen values for the gaps contribute very little to the total binding energy of the nuclei in the present model. Also, it has been shown in refs [32,33] that the standard RMF approach breaks down near the $N = Z$ nuclei region. For this reason, we have chosen here a mixed approach for pairing, i.e., taking standard BCS pairing into account for some cases and neglecting it for some other cases, depending on the situation.

Based on the above considerations, our calculated potential energy surfaces in quadrupole constraint for the $N = Z$, Ne–Ba nuclei are plotted in figures 1–7 and some of our results of free calculations (no quadrupole constraint) are given in table 1. Table 1 presents the results of our complete calculation for the ground state binding energies (BE), the first excited state solutions (the intrinsic binding energies E_{intr}), the root mean square (rms) charge radii r_c, and the quadrupole deformation parameter β_2 for all the parameter sets by considering the full pairing gaps of ref. [30]. We also display in table 1 the experimental data [31,34] and other theoretical (finite range droplet model, FRDM) predictions [35], wherever possible, for comparison. Again, we repeated the free calculations with zero pairing ($\Delta_n = \Delta_p = 0.5$ MeV). Note that by a small change in Δ_n and Δ_p, (i.e. varying from 0.0 to 0.6 MeV) the calculated RMF results do not change considerably. The results for zero pairing ($\Delta_n = \Delta_p = 0.5$ MeV) for some of the selected minima are also presented (denoted by asterisks (*)) in the table. Comparing both the cases, we notice for many nuclei, the results to be similar. However, in some of the cases, like ^{20}Ne, ^{32}S, ^{44}Ti and ^{60}Zn, a small pairing or zero pairing is necessary. To get comparable results with the experimental observations, a zero pairing is preferable for all the considered nuclei. In general, our RMF results for the ground state binding energies and quadrupole deformation parameters β_2 agree well with both the experimental data and FRDM calculations. The rms charge radii r_c for all the parameter sets are similar and their values for the excited states are slightly lower, as compared to that for the ground states.

Figure 1 gives our plot of the potential energy as a function of the quadrupole deformation parameter β_2 for ^{20}Ne, ^{24}Mg, ^{28}Si and ^{32}S nuclei. We first notice that all the three parameter sets show a similar behaviour of the potential energy surfaces (PES). The ^{20}Ne and ^{24}Mg nuclei are the cases of shape isomerism (two or more deep minima at different deformations), while ^{28}Si and ^{32}S are showing the shape coexistence with an energy difference of less than 1.0 MeV. The ground state shape of ^{28}Si is oblate ($\beta_2 \simeq -0.35$) while those of the other three nuclei are prolate ($\beta_2 = 0.5$, $\simeq 0.48$ and $\simeq 0.2$ for ^{20}Ne, ^{24}Mg and ^{32}S, respectively). In the upper panel of figure 1, a well-defined excited state above the ground state for ^{24}Mg is at $\simeq 4.3$ MeV for NL3 and TM1 and at $\simeq 4.1$ MeV for NL-RA1 set. The barrier height is $\simeq 5.0$ MeV in all the three sets. In the lower panel of figure 1, the excited state of ^{28}Si is not well-defined and is rather shallow with the energy so close to the ground state that the two could be considered as degenerate solutions, for all the three parameter sets. Such solutions could vanish with a small change of the input quantities, and will be further discussed in the next section. In such diagrams, a note of caution is needed for the discussion of the shape of nuclei. It is interesting to see in figure 1 that, for ^{28}Si, the PES curve shows different form for TM1 set as compared to NL3 and NL-RA1. However, the ground state deformations are found to be almost similar in all the three sets (see table). It may happen that the
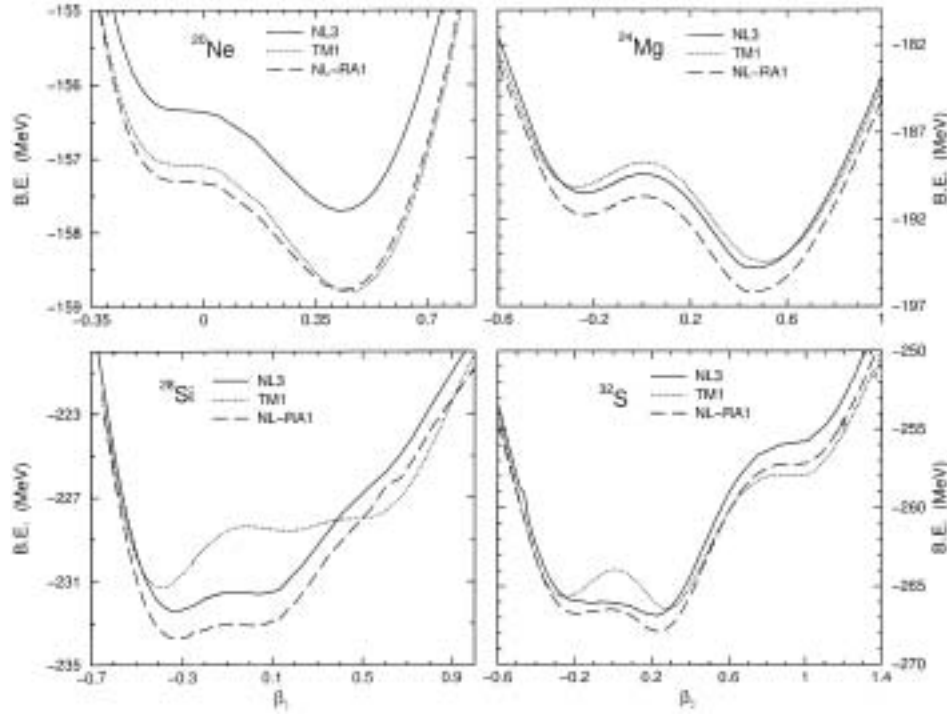
Figure 1. The RMF binding energy, calculated in a quadrupole constraint, as a function of the quadrupole deformation for ^{20}Ne, ^{24}Mg, ^{28}Si and ^{32}S, using NL3, TM1 and NL-RA1 parameter sets. The pairing strength is from ref. [30].

orientation of the nucleus is of γ-soft structure and the true shape could be obtained only in a triaxial constraint calculation [10,11,23]. As we have already mentioned in the Introduction, the shallow minima in the PES curves may not necessarily follow a solution in the free (no quadrupole constraint) calculations. Many minima in the potential energy surface curve collectively will give a stable solution for the nucleus [7]. Furthermore, while talking about the shape coexistence of the states, it is worthwhile to mention that in the coexisting energy minima in one-dimensional energy curves, caution must be taken, particularly when oblate and prolate minima have similar absolute value of β_2. Such minima may be connected by triaxial shapes and only one of them may be a real (γ-soft) minimum. This feature will become clear if a triaxial calculation (including γ-deformation) is carried out. However, in the present investigation we have not taken this point into consideration. A triaxial potential energy surface calculation in this mass region may be an interesting study in future. Similarly, in the case of ^{32}S, the well-defined excited state is shown only by TM1 set. The signatures of superdeformed state is predicted in ^{32}S at $\beta_2 \simeq 1$ which is $\simeq 8.5$ MeV above the ground state for TM1, $\simeq 10.9$ MeV for NL-RA1 and $\simeq 11$ MeV for NL3 parameter set.
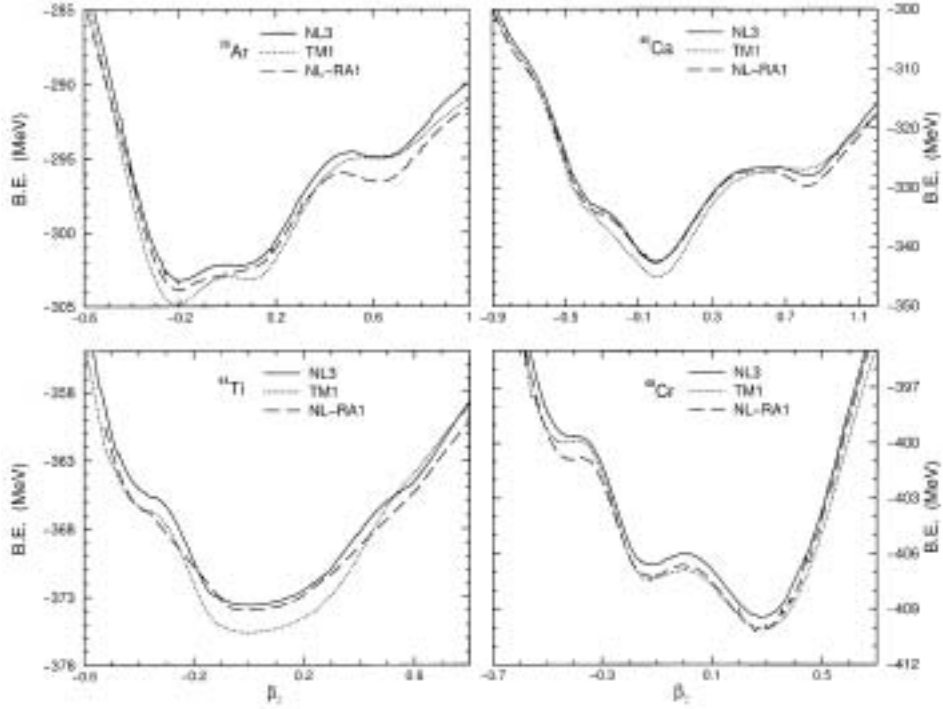
Figure 2. Same as for figure 1, but for ^{36}Ar, ^{40}Ca, ^{44}Ti and ^{48}Cr.

The potential energy surfaces (PES) for ^{36}Ar, ^{40}Ca, ^{44}Ti and ^{48}Cr are given in figure 2. The shape of ^{36}Ar in the ground state is oblate, that of ^{40}Ca and ^{44}Ti are spherical while that of ^{48}Cr is prolate. Thus, with the addition of four nucleons each, the shape changes from oblate to spherical and then from spherical to prolate. The excited states minima in these nuclei are relatively shallower, different for different parameter sets. For ^{36}Ar, an isomeric excited state is predicted at $\beta_2 \simeq 0.62$ or 0.64 for NL3 or NL-RA1 parameter set, in agreement with the recent experiment [12] (β_2(expt.) $= 0.65$). The same is true for TM1, but the minima is shallower in this case. The excitation energy above the ground state is about 8.1 MeV for NL3, 10 MeV for TM1 and 7.5 MeV for NL-RA1 parameter set. There is also a small local minimum at $\beta_2 \simeq 0.13$ for all the three parameter sets. ^{40}Ca is a double closed shell nucleus, and hence the PES shows a deep spherical minimum. Another minimum at $\simeq 15$ MeV or $\simeq 18$ MeV above the ground state is seen at $\beta_2 \simeq 0.81$ for NL3 or NL-RA1 set, respectively, whereas the same is $\simeq 18$ MeV higher at $\beta_2 \simeq 0.9$ (hence, the superdeformed state) for the TM1 force. Also an oblate minimum is obtained at $\beta_2 \simeq -0.45$ in NL3 and NL-RA1, which for the TM1 set is rather shallow and is like a local minimum. The PES for ^{44}Ti show identical trends for all the three forces. The (very shallow) first excited states minima in each case lie at $\beta_2 \simeq -0.38$ which is $\simeq 10$ MeV higher, for all forces. For ^{48}Cr, there is a well-defined excited state indicated by all the sets. The ground state energy is $\simeq 410.0$ MeV for TM1 and NL-RA1 and $\simeq 409.5$ MeV for NL3, all at $\beta_2 = 0.27$. The first excited state
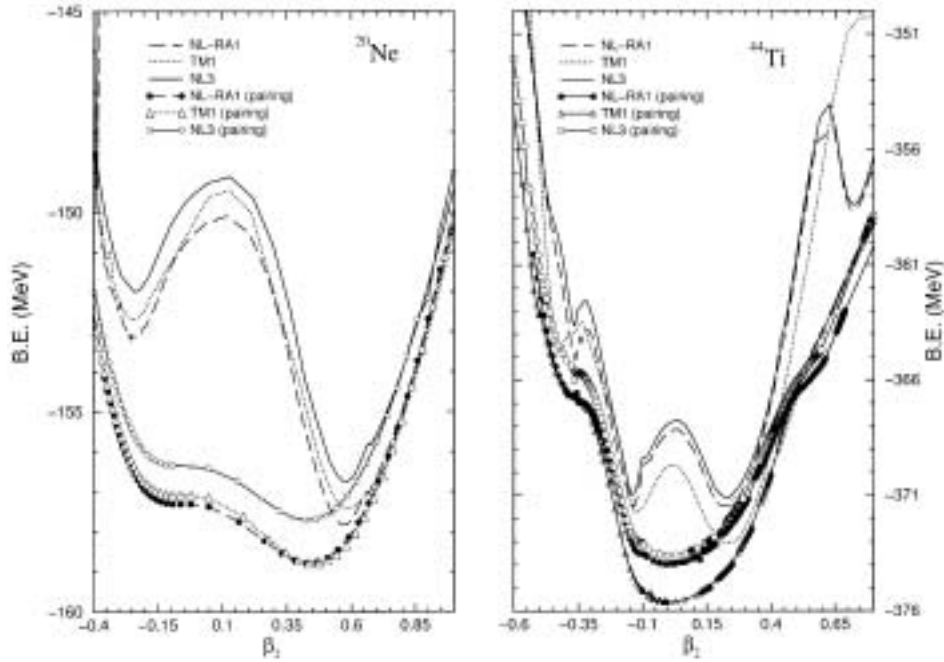
Figure 3. Same as for figure 1, but for ^{20}Ne and ^{44}Ti, and with and without pairing.

is $\simeq 2$ MeV above the ground-state with an oblate deformation of $\beta_2 = -0.11$. Once again, like for ^{36}Ar, there is a shape coexistence for ^{48}Cr. Therefore ^{36}Ar and ^{48}Cr are the clear cases of shape coexistences, with two nearly equally deep minima at different deformations in the PES. It is to be noted here that in our earlier investigation [1] for the mass region $A \simeq 80$ (specifically, for ^{72}Kr to ^{92}Pd nuclei), we get multiple shape structures in PES for all nuclei. There is always a competition between prolate and oblate solutions in the ground state of these nuclei. We know that, in general, the prolate configuration has a larger moment of inertia than the oblate one, and the upper part of the g-band of even–even nuclei can be expected to have a prolate shape although in some nuclei the ground state itself could correspond to an oblate or spherical shape [2]. The oblate-shaped rotational bands appear low in energy, when the excitation of some quasi-particles is involved. Another important observation, evident from figure 2, is the minima in the PES at about $\beta_2 \simeq -0.2$ in the case of ^{36}Ar for all the parameter sets. If one looks at the free solutions in table 1, the minimum for ^{36}Ar is at $\beta_2 \simeq -0.16$, a value slightly smaller than in figure 2 mentioned above. This happens due to the influence of the lower shallow minima appearing in the PES curve, which are not considered in the free solution [7]. Finally, it may be mentioned here that in PES, pairing plays a very important role in some of the cases, like for ^{20}Ne and ^{44}Ti illustrated in figure 3. In this figure, the PES curve with and without pairing is compared and we find a large difference between these two results. If the pairing is
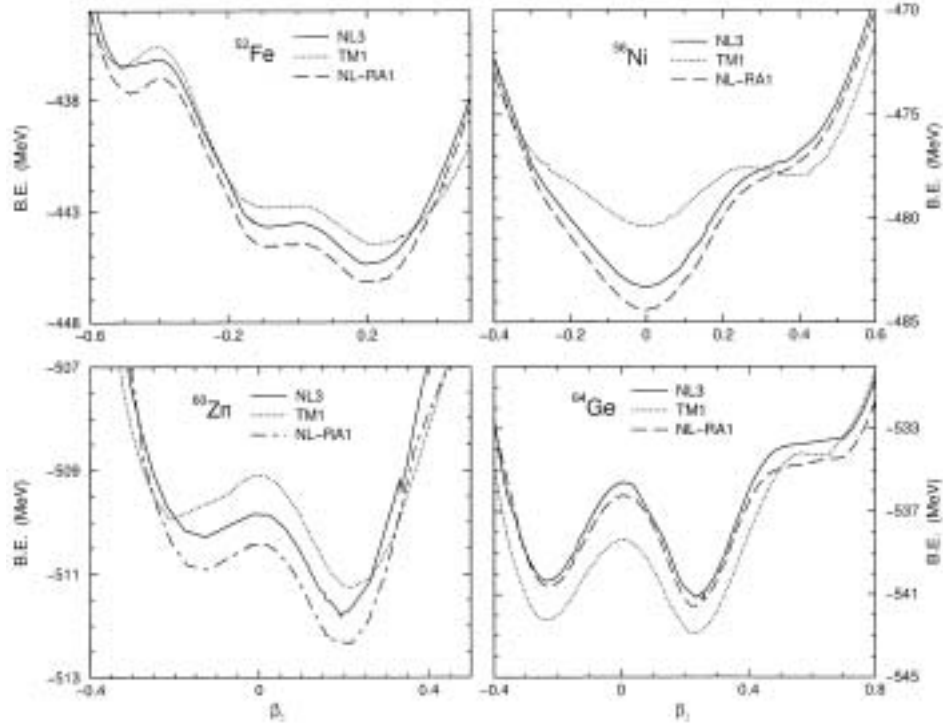
Figure 4. Same as for figure 1, but for ^{52}Fe, ^{56}Ni, ^{60}Zn and ^{64}Ge.

included, then it is not possible to obtain the ground state minimum at the right position to reproduce the experimental value of the ground deformation. However, for zero pairing interaction in figure 3, the predicted β_2 value agrees well with the experimental value (see also figures 1 and 2).

The PES for ^{52}Fe, ^{56}Ni, ^{60}Zn and ^{64}Ge are plotted in figure 4 and show that all the parameter sets give two distinct minima in each case (except for ^{56}Ni in cases of NL3 and NL-RA1), with energy of first excited minimum close (< 2 MeV) to ground state energy. In the case of ^{52}Fe, the oblate excited state is $\simeq 8.0$ MeV above the prolate ground state with deformation $\beta_2 \simeq -0.5$. There is also a local minimum at the height of $\simeq 2.0$ MeV, predicted by all the parameter sets. For ^{56}Ni nucleus, the two minima (spherical ground state and oblate excited state) for TM1 are separated by $\simeq 2.0$ MeV, whereas the same are rather shallow for NL3 and NL-RA1. There is distinct isomeric state, $\simeq 1.4$ MeV above the prolate ground state, in the plot of ^{60}Zn. The ground and oblate minimum for all the parameter sets is separated by a barrier height of $\simeq 2$ MeV. But in the case of ^{64}Ge the two shapes (oblate and prolate) are having the energy difference of $\simeq 0.8$ MeV only. This means that there is a clear shape coexistence in ^{60}Zn and ^{64}Ge in which all the parameter sets agree well with each other. These are the additional examples of two shape coexisting states. The large prolate minimum is, however, separated by a relatively higher barrier, $\simeq 4.5$ MeV, in ^{64}Ge for all the parameter sets.
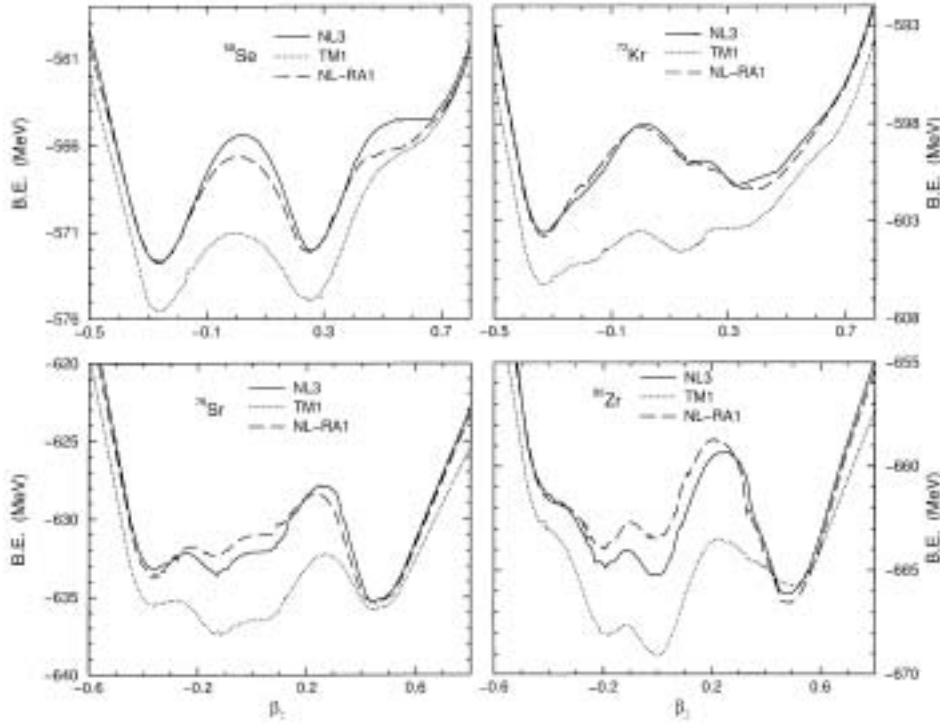
Figure 5. Same as for figure 1, but for ^{68}Se, ^{72}Kr, ^{76}Sr and ^{80}Zr.

Figures 5 and 6 give the PES for the region comprising $A = 82\pm10$ nuclei, already studied in ref. [1]. The new cases are ^{68}Se and ^{96}Cd. This region is already shown to be the interesting region of multiple shape coexistences, and ^{68}Se also presents the same result (two shape coexisting states), thereby extending this region by one unit at the beginning side. On the other hand, in ^{96}Cd all the parameter sets show the spherical ground state. Hence, adding ^{52}Fe, ^{60}Zn and ^{64}Ge from figure 4 and ^{68}Se from figure 5 to the already studied region in ref. [1], we have $A = 52$ and 60–92 as the region of (multiple) shape coexisting states. Note that, compared to the PES in ref. [1], the present calculation shows significant differences. This happens because here we use the pairing prescription of ref. [30] for evaluating the pairing gaps Δ_n and Δ_p for neutron and proton, respectively, whereas in our earlier calculation of ref. [1] we had taken $\Delta_n = \Delta_p = 0.5$ MeV which is practically equivalent to zero pairing. The inclusion of stronger pairing makes the PES curves smoother and many of the low-lying minima get washed away.

The PES for ^{100}Sn, ^{104}Te, ^{108}Xe and ^{112}Ba are shown in figure 7. Similar to the case of ^{40}Ca in figure 2, all the parameter sets predict the spherical ground state for ^{100}Sn and ^{104}Te. There is no excited state in these nuclei which could also be seen in the table. This structure of PES diagram confirms the double magic structure of ^{100}Sn. Note that ^{100}Sn represents the experimental limit of proton drip line, and hence the PES for three other nuclei beyond experimental drip line (^{104}Te, ^{108}Xe
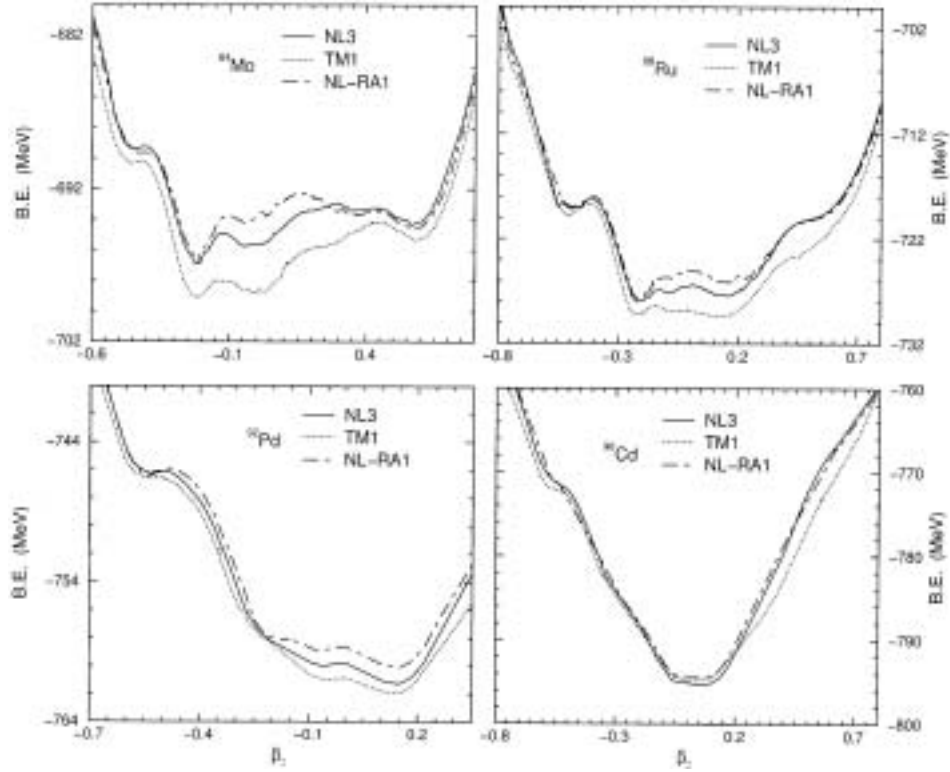
Figure 6. Same as for figure 1, but for ^{84}Mo, ^{88}Ru, ^{92}Pd and ^{96}Cd.

and ^{112}Ba) are given here simply as the theoretical predictions for completeness. The ^{108}Xe and ^{112}Ba nuclei seem to present good cases of shape coexistence for all the forces.

From the analysis of figures 1–7, we notice a qualitative difference in the PES curve for TM1, although the quadrupole deformation parameter β_2 obtained by TM1 is similar to other sets, like NL3 and NL-RA1. To be more transparent about the structure of the PES with respect to the force used, we demonstrate in figure 8, for two cases of ^{28}Si and ^{32}S, our results for the above three forces and an additional force parametrization NL-SH [36]. The behaviour of NL-SH is found to be similar to that for NL3 and NL-RA1, but different from the parametrization of TM1. Hence, the behaviour of TM1 parameter is rather unique. Due to the unique parametrizations of TM1 as discussed earlier, difference in PES is possible.

Finally, in figure 9, the difference between the ground state binding energy and the energy of the first excited state, ΔE, is presented for all the three parameter sets. Two results are apparent: (i) The shape coexistence ($\Delta E < 2.5$) nature of the solutions for all the three forces are shown for $N = Z$, ^{28}Si, ^{32}S, ^{52}Fe, ^{60}Zn, ^{64}Ge, ^{68}Se, ^{72}Kr, ^{76}Sr, ^{80}Zr, ^{84}Mo, ^{88}Ru, ^{92}Pd, ^{104}Te and ^{108}Xe nuclei. In other words, the shape coexistence region is confined mainly to the deformed $Z = 14$–16, 30–44 and 52–54 nuclei, in the vicinity of the sub-shell closure ($0d_{5/2}$) and the

Table 1. The RMF results for the binding energy (BE), the quadrupole deformation parameter (β_2), and the r.m.s. charge radius r_c of the various possible solutions for the even–even $N = Z$ nuclei. The results of the experimental (or extrapolated) data [31,34] and the micro–macroscopic finite range droplet model (FRDM) [35] are also given for comparisons. The energy is in MeV and the radius is in fm. The asterisks (*) show the calculations without pairing, i.e. $\Delta_p = \Delta_n = 0.5$. For other cases, the pairing is from ref. [30].

Nuclei	NL3 BE	NL3 β_2	NL3 r_c	TM1 BE	TM1 β_2	TM1 r_c	NL-RA1 BE	NL-RA1 β_2	NL-RA1 r_c	FRDM BE	FRDM β_2	Expt. BE	Expt. β_2	Expt. r_c
^{20}Ne	156.3	0.093	2.825	157.7	0.541	2.969	157.3	0.527	2.963	161.3	0.335	160.6	0.728	3.00
^{20}Ne*	156.7	0.531	2.975	157.9	0.541	2.969	157.8	0.526	2.963					
	152.0	−0.230	2.907	152.7	−0.234	2.904	153.1	−0.229	2.896					
^{24}Mg	194.7	0.450	3.152	194.3	0.475	3.172	196.1	0.449	3.142	198.4	0.374	198.3	0.606	3.08
	190.4	−0.200	3.112	190.0	−0.226	3.128	191.7	−0.200	3.100					
^{24}Mg*	194.4	0.485	3.045	193.6	0.516	3.080	195.7	0.486	3.042					
	187.0	−0.250	3.007	186.5	−0.287	3.038	188.4	−0.250	3.000					
^{28}Si	231.6	0.052	3.135	228.2	0.294	3.234	233.1	0.049	3.128	236.2	−0.478	236.5	0.407	3.15
	232.3	−0.289	3.197	231.2	−0.353	3.247	233.7	−0.283	3.188					
^{28}Si*	232.1	−0.329	3.125	230.9	−0.396	3.188	233.4	−0.325	3.119					
	224.0	0.575	3.293	226.4	0.595	3.289	232.9	0.008	3.021					
^{32}S	266.5	0.152	3.298	266.3	0.247	3.325	267.6	0.188	3.298	269.5	0.000	271.8	0.312	3.24
	266.1	−0.121	3.298	265.7	−0.242	3.335	266.8	−0.160	3.302					
^{32}S*	266.0	0.247	3.237	265.7	0.287	3.263	267.1	0.258	3.236					
	265.2	0.022	3.604	262.2	−0.253	3.276	265.0	−0.025	3.221					
^{36}Ar	302.5	−0.207	3.380	304.2	−0.219	3.379	303.2	−0.211	3.373	306.1	0.000	306.7	0.273	3.42
^{36}Ar*	302.5	−0.207	3.380	304.2	−0.219	3.379	303.2	−0.210	3.376					
	299.2	0.095	3.370	300.7	0.065	3.357	299.3	0.099	3.369					
^{40}Ca	342.5	0.003	3.513	345.2	0.003	3.657	342.2	0.000	3.607	342.6	0.000	342.1	0.122	3.48
^{40}Ca*	342.0	0.000	3.471	344.7	0.000	3.458	342.2	0.000	3.468					
	331.2	−0.330	3.513	332.9	−0.335	3.517	332.4	−0.331	3.508					
^{44}Ti	373.6	0.005	3.602	375.6	0.005	3.597	374.0	−0.005	3.598	376.8	0.000	375.5	0.262	3.59
^{44}Ti*	371.1	0.204	3.581	373.2	0.212	3.579	371.6	0.203	3.577					
	370.0	−0.117	3.558	371.7	−0.118	3.555	370.4	−0.119	3.555					
^{48}Cr	409.3	0.245	3.688	410.0	0.248	3.696	409.9	0.243	3.684	411.2	0.000	411.5	0.335	3.66
	406.4	−0.072	3.663	407.2	−0.063	3.668	407.0	−0.074	3.658					

Nucleus													
^{48}Cr*	408.7	0.300	3.662	409.2	0.310	3.674	409.3	0.298	3.659	447.7	0.000	447.7	0.378
	403.5	−0.146	3.627	404.0	−0.149	3.637	404.2	−0.147	3.625				
^{52}Fe	445.4	0.204	3.735	444.4	0.228	3.761	446.1	0.190	3.728				
	443.7	−0.051	3.707	442.8	−0.048	3.727	444.5	−0.043	3.703				
^{52}Fe*	444.6	0.225	3.696	443.4	0.237	3.721	445.5	0.223	3.694				
	440.5	−0.110	3.676	439.4	−0.114	3.699	441.3	−0.108	3.675				
^{56}Ni	483.3	0.004	3.759	480.4	−0.005	3.793	484.4	0.004	3.769	484.0	0.000	484.5	0.194
	483.1	0.001	3.711	479.9	0.001	3.749	484.2	−0.002	3.713				
^{56}Ni*	475.9	0.396	3.868	477.2	0.410	3.881	476.4	0.398	3.867				
^{60}Zn	511.4	0.161	3.886	511.3	0.214	3.916	512.1	0.160	3.884	515.0	0.180	514.4	0.294
	510.0	−0.067	3.877	510.0	−0.144	3.906	510.7	−0.069	3.877				
^{60}Zn*	510.9	0.222	3.860	510.5	0.231	3.884	511.6	0.221	3.860				
	507.1	−0.172	3.861	507.8	−0.185	3.882	508.1	−0.167	3.858				
^{64}Ge	541.1	0.226	3.998	542.8	0.229	4.007	541.5	0.225	3.995	546.0	0.219	544.6	0.288
	540.3	−0.217	4.005	542.2	−0.221	4.013	540.6	−0.211	4.002				
^{64}Ge*	538.8	0.231	3.969	541.3	0.229	3.978	539.6	0.228	3.966				
	537.9	−0.234	3.981	539.8	−0.236	3.989	538.2	−0.230	3.977				
^{68}Se	572.2	0.241	4.090	574.8	0.238	4.093	572.1	0.243	4.089	576.4	0.240	575.8	0.276
	572.7	−0.254	4.100	575.5	−0.250	4.101	572.7	−0.253	4.098				
^{68}Se*	571.4	0.249	4.070	574.1	0.253	4.074	571.6	−0.260	4.076				
	571.8	−0.263	4.078	574.6	−0.261	4.079	571.3	0.250	4.070				
^{72}Kr	601.1	0.313	4.181	604.5	0.139	4.147	601.4	0.351	4.187	607.1	−0.349	607.0	0.283
	603.4	−0.305	4.189	605.9	−0.290	4.188	603.6	−0.310	4.189				
^{72}Kr*	598.2	−0.189	4.143	602.2	−0.172	4.135	602.7	−0.338	4.175				
	602.5	−0.339	4.176	605.1	−0.342	4.184	599.9	0.391	4.178				
^{76}Sr	635.4	0.467	4.293	636.0	0.469	4.309	635.7	0.466	4.290	638.1	0.421	638.7	0.438
	633.4	−0.139	4.221	637.4	−0.126	4.214	633.4	−0.335	4.268				
^{76}Sr*	634.6	0.479	4.272	635.1	0.490	4.294	634.8	0.479	4.273				
	631.5	−0.376	4.263	633.4	−0.387	4.283	632.0	−0.377	4.263				
^{80}Zr	666.1	0.484	4.368	669.1	0.000	4.270	666.5	0.484	4.366	669.8	0.433	669.3	0.391
	665.3	0.000	4.275	668.0	−0.168	4.283	663.8	−0.192	4.286				
^{80}Zr*	664.0	0.000	4.264	667.7	0.000	4.256	665.7	0.488	4.338				
	665.4	0.488	4.336	664.3	0.507	4.371	662.1	−0.196	4.268				
^{84}Mo	695.7	0.000	4.328	698.8	0.000	4.327	693.9	0.000	4.328	700.9	0.053	697.0	0.299
	696.7	−0.206	4.344	699.0	−0.202	4.349	696.1	−0.209	4.343				

Table 1. (continued)

| Nuclei	NL3 BE	NL3 β_2	NL3 r_c	TM1 BE	TM1 β_2	TM1 r_c	NL-RA1 BE	NL-RA1 β_2	NL-RA1 r_c	FRDM BE	FRDM β_2	Expt. BE	Expt. β_2	Expt. r_c
^{84}Mo*	695.1	−0.220	4.328	697.4	−0.221	4.336	694.6	−0.220	4.328					
	691.2	0.234	4.327	693.3	0.230	4.336	692.1	0.336	4.340					
^{88}Ru	727.1	0.080	4.374	728.8	0.008	4.376	725.9	0.105	4.376	728.6	0.053	731.4		
	727.9	−0.199	4.391	729.0	−0.195	4.403	727.6	−0.201	4.391					
^{88}Ru*	725.7	0.152	4.373	727.4	0.152	4.380	726.2	−0.213	4.377					
	726.4	−0.214	4.376	727.5	−0.217	4.393	719.0	0.484	4.494					
^{92}Pd	761.0	0.101	4.416	761.5	0.085	4.428	759.8	0.103	4.417	760.6	0.053	762.1		
	759.8	−0.029	4.410	760.8	−0.011	4.422	761.1	−0.031	4.410					
^{92}Pd*	759.6	0.154	4.410	760.1	0.155	4.424	758.5	0.153	4.412					
	756.2	−0.190	4.410	755.8	−0.195	4.436	756.2	−0.188	4.411					
^{96}Cd	795.3	0.000	4.446	794.8	0.002	4.460	794.4	0.002	4.447	793.2	0.045	793.4		
^{96}Cd*	793.8	0.102	4.439	792.9	0.103	4.461	793.0	0.102	4.441					
	787.5	−0.153	4.430	793.9	0.111	4.460	790.7	−0.045	4.434					
^{100}Sn	830.3	0.001	4.489	828.0	0.001	4.517	829.4	0.001	4.492	825.9	0.009	824.9		
^{100}Sn*	830.0	0.000	4.465	827.6	−0.000	4.495	829.4	0.001	4.468					
^{104}Te	850.8	0.000	4.569	851.1	0.003	4.590	849.9	0.003	4.571	848.1	0.045			
^{104}Te*	849.3	0.129	4.563	849.6	0.125	4.584	848.4	0.125	4.564					
	847.9	−0.089	4.554	848.9	−0.090	4.575	847.1	−0.087	4.557					
^{108}Xe	873.4	0.161	4.660	876.0	0.152	4.672	872.3	0.156	4.660	870.8	0.152			
^{108}Xe*	871.0	−0.097	4.651	874.2	−0.081	4.662	870.1	−0.089	4.651					
	871.9	0.181	4.647	874.9	0.174	4.660	871.0	0.176	4.647					
	868.5	−0.141	4.642	871.7	−0.118	4.651	867.6	−0.128	4.639					
^{112}Ba	896.6	0.217	4.739	900.2	0.181	4.742	895.0	0.212	4.739	894.9	0.207			
^{112}Ba*	893.7	−0.165	4.733	898.5	−0.082	4.726	892.3	−0.148	4.729					
	895.2	0.240	4.731	898.1	0.235	4.741	893.4	0.238	4.732					
	887.9	−0.396	4.841	891.0	−0.398	4.854	887.0	−0.394	4.841					
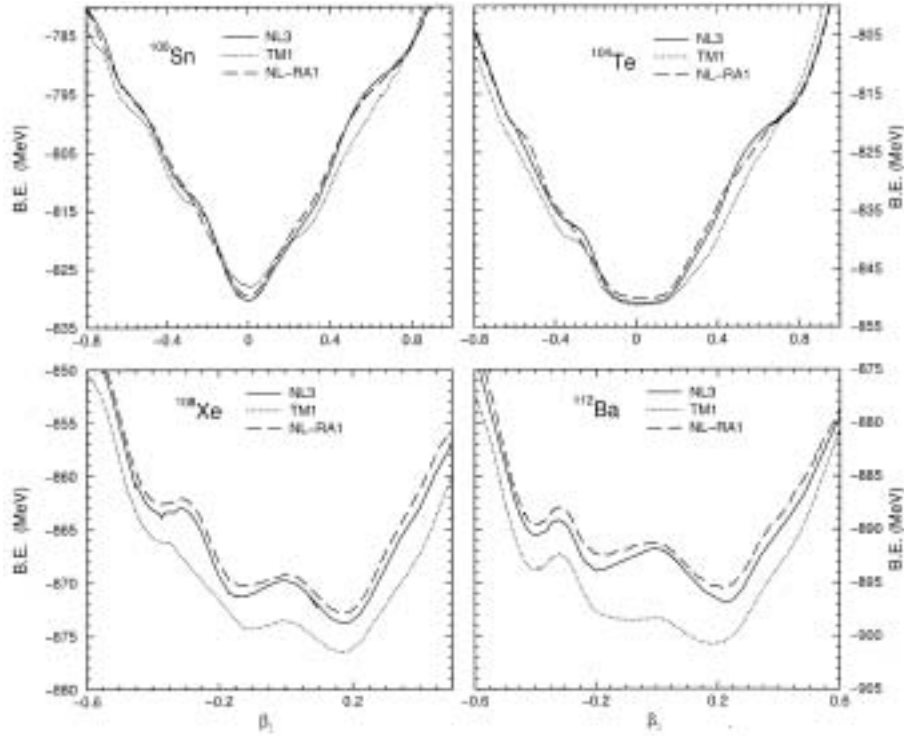
Figure 7. Same as for figure 1, but for ^{100}Sn, ^{104}Te, ^{108}Xe and ^{112}Ba.

magic numbers 28 and 50. It may be noted, however, that the shape coexistence, in the cases where excited states minima are shallow, are likely to be affected by the dynamical effects such as quadrupole vibrations. In the free calculations, in a few cases like ^{20}Ne, ^{36}Ar, ^{40}Ca, ^{44}Ti, ^{56}Ni, ^{96}Cd, ^{100}Sn and ^{104}Te nuclei, we do not find the excited states, when the pairing interaction is added. In other words, we get the finite value of ΔE for all the above-mentioned cases when the pairing interaction is small or switched off. This is shown in figure 9 for $\Delta_p = \Delta_n = 0.5$ (dotted line) for NL3 force only. Thus, in figure 9, the open circles, rectangular boxes and the open triangles lying on the zero line means the nuclei having no excited states, and we have put $\Delta E = 0$ considering that the excited state has the same binding energy as the ground state solution, which means that the pairing interaction washes away the excited state minima. On the other hand, if the pairing is off then the shape coexistence can be seen in the nuclei ^{28}Si, ^{32}S, ^{44}Ti, ^{64}Ge, ^{68}Se, ^{72}Kr and ^{104}Te. (ii) For all the parameter sets, ΔE shows the peaking structure (large value of ΔE) at all the magic numbers 20, 28 and 50. The role of pairing is once again evident from this figure, if we compare the solid line for stronger pairing with the dotted line for the case of no pairing, plotted for NL3 parameter set. The peaking structure of magic nuclei are intact for both with and without pairing correlations. Hence, the magicity of the numbers 20, 28 and 50 seems not to be affected by the pairing interaction.
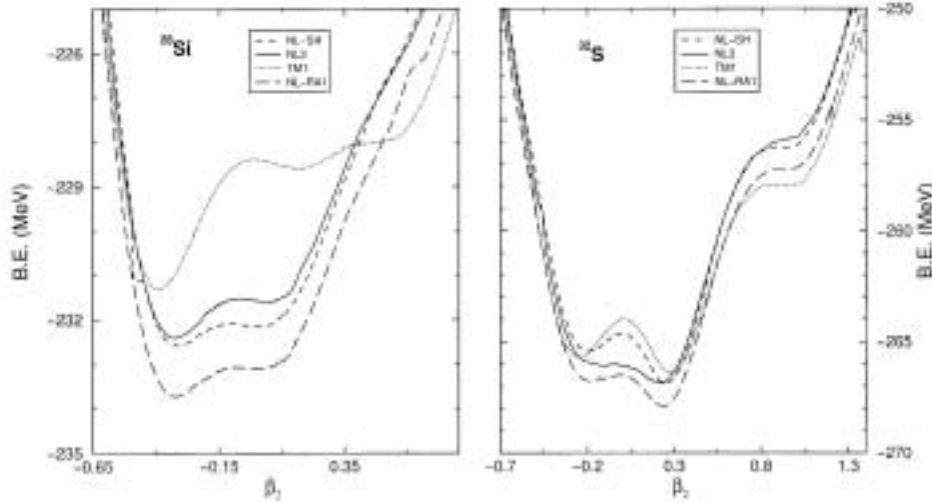
Figure 8. Same as for figure 1, but for ^{28}Si and ^{32}S, and with the additional NL-SH parameter set.

4. Summary and discussion of results

In summary, we have calculated the ground state properties of $Z = 10$ to $Z = 56$, even–even $N = Z$ nuclei, in an axially deformed relativistic mean field formalism. The parameter sets used are the NL3, TM1 and NL-RA1. Also, the whole of potential energy surfaces are determined in a quadratic constraint calculation, whose analysis of the different minima give quadrupole deformation parameters and excited state energies. In most of the nuclei ($Z = 30$–44) considered, we predict two or even three minima at various different quadrupole deformations. In the present calculations, all the three parameter sets predict qualitatively similar results for almost all the nuclei, except for some isolated systems like ^{28}Si, ^{32}S and ^{56}Ni. For example, in ^{28}Si the prolate excited minimum is at $\simeq 2.5$ MeV for TM1 whereas in the other two sets it is at less than 1.0 MeV. The region of multiple shape coexistence is found to occur mainly for the deformed $A = 68$–92 and $A = 108$, 112 nuclei. Here, two or more different solutions are found to have (nearly) the same energy. We have also compared our PES diagrams obtained with and without pairing and found that the pairing has a large effect in some cases. With the inclusion of pairing interaction, the PES curves become smoother than the curves obtained without pairing. The shallow low minima do not appear when the pairing interaction is included, while many minima are predicted when the pairing interaction is switched off [1]. An analysis of ΔE, the energy differences between ground state and first excited state solutions, show that in general all parameter sets predict correct magic shells at $N = Z = 20$, 28 and 50. The subshell closures at $N = Z = 14$ and 40 do not show any significant large value of ΔE.
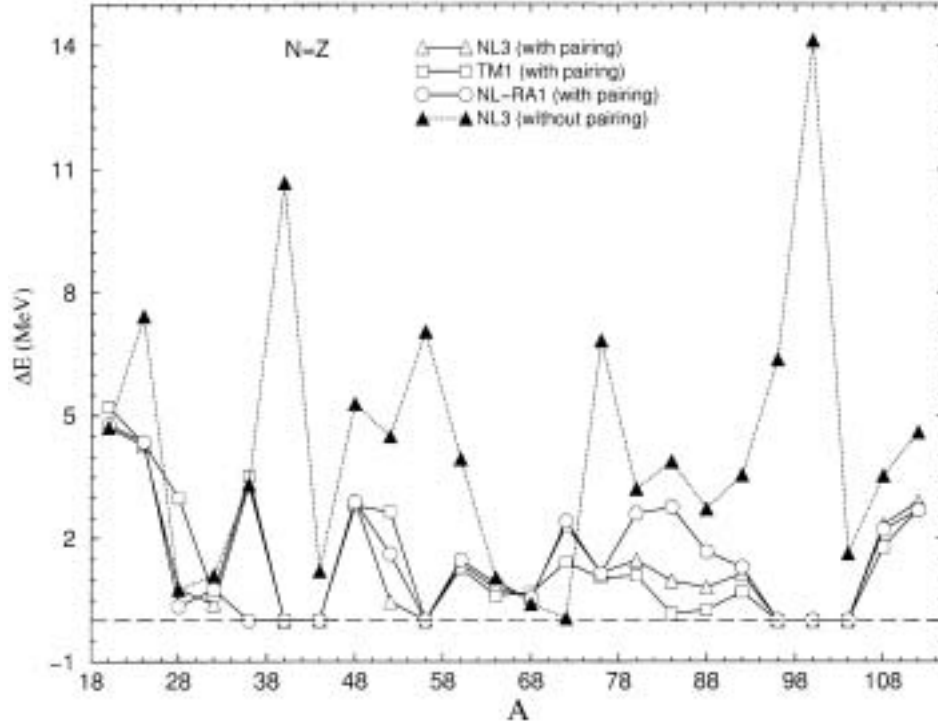
Figure 9. The difference between the RMF ground-state binding energy and the energy of the first excited state, ΔE, as a function of A for the considered $N = Z$ nuclei, for the three parameter sets. The solid lines are for the strong pairing [30] whereas the dashed line is for no pairing ($\Delta_p = \Delta_n = 0.5$).

Finally, there are some limitations of the present calculations. For example, the correlations that we have not taken into account here, are the angular momentum projection or correlations beyond the mean field (like the fluctuations) which may easily shift the value of ΔE by several hundred keV. Therefore, in order to avoid ambiguities in the predictions of ground state shapes for the shape coexisting nuclei, a more sophisticated approach for calculating the binding energies is called for. In this connection, the Dirac–Hartree–Bogoliubov approach is a prescription which treats the pairing effects in a slightly more proper way [37,38]. But it is not sure whether the relativistic Dirac–Hartree–Bogoliubov (RDHB) approach is suitable for the exotic nuclei or not, as this is also a highly parameterized calculation. Unless the Lagrangian contains the terms like $\psi\psi$, $\psi^\dagger\psi^\dagger$, $\psi^\dagger\psi^\dagger\psi\psi$ or the higher orders, we cannot say that proper pairing effects have been taken into account. In one of our earlier work [39], we have shown that the position of the orbital and the quality of binding energy predictions remain unchanged both in the relativistic Hartree approximation and relativistic Dirac–Hartree–Bogoliubov approach [38]. Thus to take pairing into account the relativistic Hartree–Bogoliubov (RHB) approach is not enough, rather a self-consistent approach which includes the relativistic Lagrangian level is very important. The improved BCS, i.e., the inclusion of quasi-bound state

is the next step in this regard [39]. In an earlier calculation [39] we have used this approach for spherical open-shell nuclei and it works remarkably well. Thus, it will be an interesting improvement if one could include the quasi-bound state for deformed calculations [40]. The energy of the 0^+ state (ground state for even–even nuclei), coming from an intrinsic configuration with large deformation, needs a special comment. A deformed intrinsic state is a superposition of various angular momentum states and, after angular momentum projection, the ground state is lowered in energy as compared to the intrinsic state E_{intr}. This lowering is large for configurations with large β values [40]. Apparently, E_{intr} can be identified with E_0 only for spherical solutions (containing only 0^+ state). However, in the present work angular momentum projection is not considered. In other words, we are concerned here only with bulk properties, such as the binding energies, nuclear deformations and the average properties of the intrinsic states and not with the spectroscopy of the bands in the studied nuclei. To project out onto good angular momentum states is an interesting problem for future investigations of the relativistic mean field model.

Acknowledgements

References

[1] S K Patra, B K Raj, M S Mehta and R K Gupta, *Phys. Rev.* **C65**, 054323 (2002)
[2] W Nazarewicz, J Dudek, R Bengtsson, T Bengtsson, and I Ragnarsson, *Nucl. Phys.* **A435**, 397 (1985)
[3] C J Lister, P J Ennis, A A Chishti, B J Varley, W Gelletly, H G Price and A N James, *Phys. Rev.* **C42**, R1191 (1990)
[4] W Gelletly, M A Bentley, H G Price, J Simpson, C J Gross, J L Durell, B J Varley, O Skeppstedt and S Rastikerdar, *Phys. Lett.* **B253**, 287 (1991)
[5] C Chandler *et al*, *Phys. Rev.* **C61**, 044309 (2000)
[6] J L Wood, K Hyde, W Nazarewicz, M Huyse and P Van Duppen, *Phys. Rep.* **215**, 101 (1992)
[7] R Bengtsson and W Nazarewicz, *Z. Phys.* **A334**, 269 (1989)
[8] K Kumar, *J. Phys.* **G4**, 849 (1978)
[9] P Bonche, H Flocard, P-H Heenen, S J Krieger and M S Weiss, *Nucl. Phys.* **A443**, 39 (1985)
[10] N Tajima, S Takahara and N Onishi, *Nucl. Phys.* **A603**, 23 (1996)
[11] S Takami, K Yabana, and M Matsnu, *Phys. Lett.* **B431**, 242 (1998)
[12] C E Svensson *et al*, *Phys. Rev. Lett.* **85**, 2693 (2000)
[13] R Julin *et al*, *J. Phys.* **G27**, R109 (2001)
[14] A N Andreyev *et al*, *Nature* **405**, 430 (2000)
[15] C J Horowitz and B D Serot, *Nucl. Phys.* **A368**, 503 (1981)
B D Serot and J D Walecka, *Adv. Nucl. Phys.* **16**, 1 (1986)
[16] Y K Gambhir, P Ring and A Thimet, *Ann. Phys. (N.Y.)* **198**, 132 (1990)
S K Patra and C R Praharaj, *Phys. Rev.* **C44**, 2552 (1991)

[17] P-G Reinhard, *Rep. Prog. Phys.* **52**, 439 (1989)
[18] P K Panda, S K Patra, J Reinhardt, J A Maruhn, H Stöcker and W Greiner, *Int. J. Mod. Phys.* **E6**, 307 (1997)
[19] H Flocard, P Quentin and D Vautherin, *Phys. Lett.* **B46**, 304 (1973)
[20] W Koepf and P Ring, *Phys. Lett.* **B212**, 397 (1988)
[21] J Fink, V Blum, P-G Reinhard, J A Maruhn and W Greiner, *Phys. Lett.* **B218**, 277 (1989)
[22] D Hirata, H Toki, I Tanihata and P Ring, *Phys. Lett.* **B314**, 168 (1993)
[23] M Yamagami, RIKEN Report No. 39 (September, 2001)
[24] Y Sugahara and H Toki, *Nucl. Phys.* **A579**, 557 (1994)
[25] G A Lalazissis, J König and P Ring, *Phys. Rev.* **C55**, 540 (1997)
[26] M Rashdan, *Phys. Rev.* **C63**, 044303 (2001)
[27] S K Patra, R K Gupta and W Greiner, *Int. J. Mod. Phys.* **E6**, 641 (1997)
    S K Patra, C-L Wu, C R Praharaj and R K Gupta, *Nucl. Phys.* **A651**, 117 (1999)
[28] A V Afanasiev, T L Khoo, S Frauendorf, G A Lalazissis and I Ahamad, *Phys. Rev.* **C67**, 024309 (2003)
[29] S Gmuca, *J. Phys.* **G17**, 1115 (1991); *Nucl. Phys.* **A547**, 447 (1992)
[30] D G Madland and J R Nix, *Nucl. Phys.* **A476**, 1 (1988)
[31] S Raman *et al*, *At. Data Nucl. Data Tables* **36**, 1 (1987)
    S Raman, C W Nestor Jr. and P Tikkanen, *At. Data Nucl. Data Tables* **78**, 1 (2001)
[32] S K Patra *et al*, *Mod. Phys. Lett.* **A13**, 2743 (1998)
    T R Werner, J A Sheikh, W Nazarewicz, M R Strayer, A S Umar and M Misu, *Phys. Lett.* **B335**, 259 (1994)
    T R Werner *et al*, *Nucl. Phys.* **A597**, 327 (1996)
[33] G A Lalazissis, D Vretenar, W Pöschl and P Ring, *Nucl. Phys.* **A632**, 363 (1998)
[34] G Audi, O Bersillon, J Blachot and A H Wapstra, *Nucl. Phys.* **A624**, 1 (1997)
[35] P Möller, J R Nix, W D Myers and W J Swiatecki, *At. Data Nucl. Data Tables* **59**, 185 (1995)
    P Möller, J R Nix and K-L Kratz, *At. Data Nucl. Data Tables* **66**, 131 (1997)
[36] M M Sharma, M A Nagarajan and P Ring, *Phys. Lett.* **B312**, 377 (1993)
[37] G A Lalazissis, D Vretenar and P Ring, *Nucl. Phys.* **A650**, 133 (1999)
    J Meng, *Nucl. Phys.* **A635**, 3 (1998)
[38] J Meng and P Ring, *Phys. Rev. Lett.* **77**, 3963 (1996)
    W Pöschl, D Vretenar, G A Lalazissis and P Ring, *Phys. Rev. Lett.* **79**, 3841 (1997)
[39] S K Patra, M Del Estal, M Centelles and X Viñas, *Phys. Rev.* **C63**, 024311 (2001)
    M Del Estal, M Centelles, X Viñas and S K Patra, *Phys. Rev.* **C63** 044321, 024314 (2001)
[40] S K Patra, S Yoshida, N Takigawa, C R Praharaj and A K Rath, *Phys. Rev.* **C51**, 2248 (1995)